Comparative Medicine
Copyright 2018
by the American Association for Laboratory Animal Science

Vol 68, No 6
December 2018
Pages 461–473

Original Research

Longitudinal Evaluation of Pulmonary Arterial Hypertension in a Rhesus Macaque (*Macaca mulatta*) Model of HIV Infection

Rebecca A Tarantelli,[1] Finja Schweitzer,[1] Marc A Simon,[2] Rebecca R Vanderpool,[2] Ian Christman,[2] Emily Rayens,[1] Heather M Kling,[3] ToniAnn Zullo,[3] Jonathan P Carney,[4] Brian J Lopresti,[4] Thomas Bertero,[5] Stephen Y Chan,[2] and Karen A Norris[1,*]

Pulmonary arterial hypertension (PAH) is a life-threatening disease with higher incidence in HIV-infected compared with noninfected patients. SIV-infected NHP develop clinical manifestations of HIV infection, including PAH. To understand the pathogenesis of PAH and determine the relationship between hemodynamic changes and clinical characteristics associated with SIV infection, we performed right heart catheterization and echocardiographic imaging of 21 rhesus macaques before and after SIV infection. Between 6 and 12 mo after infection, 11 of the 21 animals had elevated mean pulmonary arterial pressure (mPAP; greater than 25 mm Hg). RV involvement was evident as increased RV glucose uptake in PAH$^+$ macaques on positron emission tomography–coupled CT compared with uninfected animals. RV and pulmonary vascular collagen deposition were elevated in PAH$^+$ animals. At 12 mo after infection, 6 of the 21 macaques (28.6%) exhibited continued increase in mPAP (progressive PAH), whereas 5 animals (23.8%) had reduced pressure (transient PAH). SIV infection of rhesus macaques led to 3 distinct outcomes with regard to hemodynamic function. Hemodynamic alterations correlated with specific inflammatory profiles and increased RV and pulmonary arterial fibrosis but not with viral load, sex, or CD4$^+$ T-cell levels. This model of a natural cause of PAH provides insight into disease pathways that are important for the development of novel therapeutic targets.

Abbreviations: BALF, bronchoalveolar lavage fluid; CCL, C-C motif chemokine ligand; CXCL, C-C-C motif chemokine ligand; FDG, 2-deoxy-2-[^{18}F]-fluoro-D-glucose; IP, IFNγ-inducible protein; LV+S, left ventricle plus septum; MDC, macrophage-derived chemokine; MIP, macrophage inflammatory protein; mPAP, mean pulmonary artery pressure; NBF, neutral buffered formalin; RHC, right heart catheterization; RV, right ventricle; SUV, standard uptake value; TGF, transforming growth factor; VEGF, vascular endothelial growth factor

DOI: 10.30802/AALAS-CM-18-000012

Although the life expectancy of HIV$^+$ persons has improved with the use of antiretroviral therapy, this population remains at increased risk for the development of noninfectious diseases including cardiovascular disease, chronic obstructive pulmonary disease and pulmonary arterial hypertension (PAH). The prevalence of PAH is increased in HIV-infected persons, although little is known regarding the pathogenesis of HIV-associated PAH (HIV–PAH).[35,36] HIV-PAH may be more common than previously thought, because recent studies of echocardiography in HIV-infected outpatients found that between 15% and 35% had elevated pulmonary artery pressures.[13,24,25] The effect of antiretroviral therapy on the prevalence or clinical outcome of PAH remains undecided, given that the prevalence of HIV-PAH has not changed appreciably in the antiretroviral therapy era.[7]

The pathogenesis of PAH remains incompletely understood, and the direct effect of HIV on the pathophysiology of HIV-associated PAH is difficult to discern. Direct detection of virus in the pulmonary vasculature has generally been unsuccessful; however in vitro and in vivo studies have suggested a role for HIV proteins in promoting endothelial and smooth muscle cell hypertrophy, suggesting a role for viral proteins in the development of pulmonary vascular stiffness and remodeling.[19,32]

An impediment to improved understanding of PAH pathogenesis is the lack of appropriate animal models that mimic human disease. Although rodent models of PAH using monocrotaline or hypoxia have increased the understanding of some aspects of PAH pathogenesis, these models do not recapitulate the direct or indirect role of HIV in the development of HIV–PAH. Infections of either SIV or SIV–HIV chimeric virus of susceptible NHP species are well characterized models of HIV infection with histopathologic evidence of naturally occurring PAH.[5,11,12,18] In addition, we previously reported that rhesus and cynomolgus macaques that are chronically infected with either SIV or HIV–SIV chimeric virus had a high prevalence of increased pulmonary artery and right heart pressures, without elevations in pulmonary capillary wedge pressure, systemic blood pressure, or increased cardiac output.[12] Together, these studies point to SIV-infected macaques as a model of HIV-associated PAH that is highly relevant for discerning the pathogenic

Received: 30 Jan 2018. Revision requested: 17 Mar 2018. Accepted: 30 Jun 2018.
[1]Center for Vaccine and Immunology, University of Georgia, Athens, Georgia; [2]Vascular Medicine Institute and Departments of [3]Immunology and [4] Radiology, University of Pittsburgh, Pittsburgh, Pennsylvania; and [5]Institute for Research on Cancer and Aging, Université Côte d'Azur, Nice, France
[*]Corresponding author. Email: kanorris@uga.edu

process without confounders, such as antiretroviral therapy and intravenous drug use, or the need for additional inducers, such as monocrotaline.

In the present study, we have developed novel assessment protocols for the longitudinal evaluation of cardiopulmonary function in SIV-PAH primates, including serial right heart catheterization (RHC), serial echocardiography, and serial assessment of inflammatory mediators in plasma and brochoalveolar lavage fluid (BALF). In addition, we have developed right-heart metabolic evaluation by using co-registered position emission tomography (PET-CT) to evaluate alterations in the cardiac metabolic state, which we completed at study termination on subsets of naïve and SIV-infected macaques. The longitudinal nature of these studies revealed the development of early elevated pulmonary arterial and right ventricular (RV) pressures in a subset of SIV-infected macaques. We further show that SIV-PAH can be progressive in a subset of these animals, with worsening hemodynamic profile over time, or transient, with pulmonary and RV pressures returning to near-baseline levels by 12 mo after infection. We investigated the relationship of hemodynamic derangement with SIV disease progression, right heart metabolic alterations, and systemic and pulmonary inflammation and fibrosis.

Materials and Methods

Animals and study design. The study population comprised of 21 (12 male, 9 female) Chinese rhesus macaques (*Macaca mulatta*), which had been obtained from approved vendors or national primate centers and housed in accordance with the *Guide for the Care and Use of Laboratory Animals*[14] under the direction of the Department of Laboratory Animal Research (University of Pittsburgh, PA). Studies were approved by the IACUC at the University of Pittsburgh. Prior to study initiation, all 21 macaques underwent complete clinical and physical evaluations. At baseline assessments, macaques were excluded from the study when the pulmonary arterial pressure was at least 25 mm Hg or they had evidence of pulmonary or cardiac abnormalities.

SIV infection. Macaques were sedated by using ketamine (10 to 15 mg/kg IM). Once animals were sedated, an intravenous catheter was placed, and SIV ΔB670 ($TCID_{50}$, 2.6×10^5; 1:100 dilution of viral stock) was administered. In addition, a subset of animals (female, $n = 9$) received mucosal exposure of SIV ΔB670 ($TCID_{50}$, 2.6×10^4) through rectal wash. Throughout infection, serial blood and BALF samples were obtained for assessment of viral load and flow cytometric analysis. At the completion of the study (10 to 12 mo after infection), macaques were humanely euthanized, and tissues samples were collected for morphometric analysis.

RHC. All procedures in this study were completed by a single operator, who has performed more than 100 RHC procedures in rhesus macaques. RHC was performed at baseline (before infection), 6 mo after infection, and prior to study termination (10 to 12 mo after infection). Animals were sedated by using ketamine (10 to 15 mg/kg IM). Peripheral blood pressure was acquired by using a pediatric aneroid sphygmomanometer (Lumeon, Boston, MA) over the brachial artery. An intravenous catheter was placed in the saphenous vein, and Lactated Ringer solution was administered at 1 drop every 10 s throughout the procedure. Macaques were intubated with a 4.5 to 6 French endotracheal tube and brought to a surgical plane of anesthesia maintained on 1.5% isoflurane. Animals were placed in Trendelenburg position; the surgical site was clipped and aseptically scrubbed with alternating chlorhexidine and alcohol scrub; and covered with a fenestrated drape. By using a 5-French transradial artery access kit (Arrow, Morrisville, NC), the internal jugular–subclavian venous junction was punctured. After guide wire insertion, a 1- to 2-mm incision was made in the skin to ease insertion of the 5-French introducer (Avanti, Arrow). For pressure evaluation, a 5-French Swan–Ganz balloon wedge pressure catheter (Arrow) was advanced through the right atrium, right ventricle, and pulmonary artery. Pressures were recorded (M100 Acquisition system, Biopac, Goleta, CA). All data were collected within 45 min of sedation to reduce the effect of anesthetic on pressure variance. After waveform recordings were completed, the catheter was removed, and direct pressure was applied to the insertion site for a minimum of 5 min. Cefazolin (25 mg/kg IM) was administered once prophylactically.

Waveforms were evaluated, and mean values (right ventricular systolic pressure, right ventricular diastolic pressure, right ventricular end-systolic pressure, right atrial pressure, and pulmonary arterial pressure [PAP]) were obtained from 3 to 5 recorded beats per parameter. When the pulmonary artery could not be accessed directly during RHC, mean PAP (mPAP) was calculated as described previously:[38]

$$\text{mPAP (in mm Hg)} - 0.65 \times (\text{right ventricular systolic pressure}) + 0.55$$

The mPAP calculation was validated by using 7 normal macaques (direct mPAP of 15.15 mm Hg compared with calculated mPAP of 17.37 mm Hg, $P = 0.1$).

Echocardiographic imaging. Echocardiographic imaging was completed at baseline, 6 mo after infection, and at study end. The macaques underwent an overnight fast and were sedated by using ketamine (10 to 15 mg/kg IM). The animals were placed in dorsal recumbency, and cardiac images were captured (Vivid I ultrasound machine, GE Healthcare, Chicago, IL).

Positron emission tomography. After an overnight fast, macaques were lightly sedated by using ketamine (2 to 5 mg/kg IM) and then injected intravenously with 10 mCi 2-deoxy-2-[^{18}F]-fluoro-D-glucose (FDG). After a 3-h uptake period, macaques were sedated with ketamine (10 to 15 mg/kg IM) and maintained at a surgical plane of anesthesia by using 1.5% isoflurane throughout the CT and positron emission tomography (PET) scans. IV patency was maintained by instilling Lactated Ringers solution at 1 drop every 10 s.

Animals were scanned for 50 min by using a mobile neurologic CT scanner (Neurologica CereTom, Danvers, MA) combined with a microPET scanner (P4, Siemens, Cary, NC) for inline PET–CT imaging. CT images were used for precise positioning of the heart within the 8-cm PET axial field of view and for attenuation correction and localization. Standard uptake values (SUV) were obtained by isolating a 0.3-cm^2 region of interest (https://www.osirix-viewer.com/) over the right ventricle (RV) and left ventricle (LV). Standardization landmarks were chosen between approximately the 7th and 9th thoracic vertebra. SUV were obtained for each slice, and mean values were calculated between these landmarks. SUV is expressed as an RV:LV ratio.

Tissue morphometric analysis. At necropsy, heart and lung were collected and preserved for analysis. The complete right lung was inflated at 20 cm of gravitational pressure by using 10% neutral buffered formalin and submerged in 10% neutral buffered formalin for a minimum of 3 wk. Once fixed, lung tissue was cut into approximately 1.5×1.5-cm sections. Random tissue sections were cut and including 3 sections from upper lobes, 2 from the middle lobe, and 3 from lower lobes.

The RV and LV including septum (LV+S) were collected at necropsy. Each was weighed by using a gram scale to calculate

Cytokines	Chemokines	Growth factors	Acute-phase protein
IL1β	Eotaxin/CCL11	EGF	C-reactive protein
IL1RA	IL8	FGF-basic	
IL2	MCP1/CCL2	HGF	
IL4	MDC/CCL22	VEGF	
IL5	MIF	TGFβ	
IL6	MIG/CXCL9		
IL10	MIP1α/CCL3		
IL12	MIP1β/CCL4		
IL15	ITAC/CXCL11		
IL17	RANTES/CCL5		
G-CSF			
GM-CSF			
IFNγ			
IP10/CXCL10			
TNFα			

Figure 1. Cytokines, chemokines, growth factors, and acute phase protein quantified in longitudinal plasma and BALF samples from 22 SIV-infected rhesus macaques. CCL, C-C motif chemokine ligand; CXCL, C-X-C motif chemokine ligand; EGF, epidermal growth factor; FGF, fibroblast growth factor; G-CSF, granulocyte-colony stimulating factor; GM-CSF, granulocyte–macrophage colony-stimulating factor; HGF, hepatocyte growth factor; IP, IFNγ-inducible protein; ITAC, IFN-inducible T-cell α chemoattractant; MDC, macrophage-derived chemokine; MIF, macrophage migration inhibitory factor; MIG, monokine-induced by IFNγ; MIP, macrophage inflammatory protein; RA, receptor antagonist; RANTES, regulated on activation, normal T cell expressed and secreted; TGF, transforming growth factor; VEGF, vascular endothelial growth factor.

Fulton index (that is, RV/LV+S). Sections (1 cm each) were cut at the midpoints of the RV and LV.

Sections of heart and lung tissue were paraffin-embedded, cut at a thickness of 5 µm, and stained with hematoxylin and eosin, Mason trichrome, and picrosirius red.

To assess cardiac collagen deposition, trichrome-stained slides from the RV and LV were imaged (Application Suite version 4.4, Leica, Wetzlar, Germany). Five images of cardiac muscular tissue without vessels were captured at 20× magnification per tissue section for the RV and LV separately.

The images were analyzed by using Image J software (https://imagej.nih.gov/ij/), with the Threshold color plugin set to RGB; bright blue collagen was selected, converted to a binary image, and measured to quantify the collagen area. This process was repeated for the red-stained myocytes and measured to obtain the muscle tissue area. All 5 images were integrated, and collagen deposition results are reported as:

$$\%\ \text{collagen}\ /\ 170\ \text{mm}^2 = (\text{total collagen area})\ /\ (\text{total muscle area})\ \times\ 100\%$$

To assess lung periarteriolar collagen deposition, lung tissue slides were stained by using 0.1% picrosirius red (Direct Red80, Sigma-Aldrich, St Louis, MO) and counterstained with Weigert hematoxylin to reveal fibrillar collagen. The sections then were imaged serially by using an analyzer and polarizer oriented parallel and orthogonally to each other. Microscope conditions (lamp brightness, condenser opening, objective, zoom, exposure time, and gain parameters) were maintained throughout the imaging of all samples. A minimal threshold was set on appropriate control sections for each experiment, in which only the light passing through the orthogonally oriented polarizers representing fibrous structures (that is, excluding residual light from the black background) was included. The threshold was maintained for all images across all conditions within each experiment. The area of the transferred regions that was covered by the thresholded light was calculated, and at least 10 sections per vessel per condition were averaged together (Image J software).

To evaluate myocyte thickness, images of hematoxylin- and eosin-stained myocytes from RV and LV tissue sections at 40× magnification over 10 fields of view were obtained. Myocytes with discernable borders and cut transversely were measured across the nucleus by using ImageJ software. Mean values of 30 cells were obtained for each macaque.

Flow cytometric analysis. The following directly conjugated monoclonal antibodies were used to analyze monocytes by flow cytometry: CD3 (clone SP34)–FITC (BD Biosciences, San Jose, CA), CD4 (clone OKT4)–PE/Cy7, and CD8 (clone SK1)–BV510 (BioLegend, San Diego, CA). Raw cytometry data were acquired on a flow cytometer (LSRII, BD Biosciences) and analyzed by using FlowJo software (Tree Star, Ashland, OR). All cytometry experiments included fluorescence-minus-one controls. Doublet cells were excluded from analyses according to forward scatter-A and forward scatter-H parameters. For each experiment, the lymphocyte population was gated by using forward and side scatter. To characterize T cells, $CD3^+$ cells were analyzed on the basis of their differential expression of CD4 and CD8. Numbers of $CD4^+$ T cells were calculated according to lymphocyte numbers determined from a differential blood count.

Cytokine and chemokine analysis. Cytokines, chemokines, and growth factors (Figure 1) in plasma and BALF were quantified (Cytokine 29-Plex Monkey Panel, Invitrogen, Carlsbad, CA) according to the manufacturer's instructions. C-reactive protein and TGFβ levels were analyzed by using NHP-specific ELISA kits (Abnova, Walnut, CA, and myBioSource, San Diego, CA, respectively). The dilution effect of BALF samples was normalized according to plasma urea concentrations.[30]

Statistical analysis. All statistical analyses were completed by using Prism (version 7.00 for Windows, GraphPad Software, La Jolla, CA). The Student *t* test was used for all group comparative analysis. Repeated-measures ANOVA was used for $CD4^+$ T-cell and viral load analyses. Differences in inflammatory markers in PAH^+ compared with PAH^- macaques at 6 mo after infection and at study termination were assessed by using Mann–Whitney tests. To test for associations between mPAP and each immune marker, Spearman correlation was used. To test for associations between mPAP or right ventricular systolic pressure and each immune marker, Pearson correlation was used. For all analysis, a P value of less than 0.05 was considered significant.

Results

Study cohort and SIV infection. To establish normal hemodynamic parameters in uninfected adult rhesus macaques, we

Table 1. Clinical characteristics of SIV infected rhesus macaques

Animal	Sex	Age at infection (y)	Weight at infection (kg)	Baseline blood pressure (mm Hg)	Chronic $CD4^+$ (no. of cells/μL)	Peak viral load (no. of RNA copies/mL)	Viral set point (no. of RNA copies/mL)	Peak mPAP (mm Hg)	PAH status
2813	F	6.6	6.2	100/60	677	1.2×10^7	1.8×10^4	25.5	P-PAH$^+$
3213	F	5.3	6.4	110/70	297	2.4×10^7	2.0×10^6	27.9	P-PAH$^+$
3313	F	6.1	8.0	110/70	701	4.4×10^7	2.0×10^6	26.1	T-PAH$^+$
3413	F	4.9	5.4	120/65	440	3.9×10^7	5.9×10^5	34.7	T-PAH$^+$
10613	M	5.7	7.2	130/80	449	3.8×10^6	3.3×10^6	31.1	P-PAH$^+$
11613	M	5.9	7.4	130/80	447	1.2×10^8	2.2×10^6	26.3	P-PAH$^+$
17511	M	7.3	11.8	140/80	413	4.8×10^6	3.5×10^4	37.3	T-PAH$^+$
17611	M	7.1	10.8	120/70	128	1.1×10^7	1.1×10^6	25.2	P-PAH$^+$
18011	M	7.9	10.2	110/50	733	2.6×10^6	2.1×10^5	36.5	P-PAH$^+$
18211	M	8.3	12.4	130/90	372	1.0×10^7	1.3×10^6	32.0	T-PAH$^+$
18311	M	7.2	11.6	110/50	443	7.3×10^6	9.6×10^5	27.5	T-PAH$^+$
Mean ± SEM		6.6 ± 0.3	8.9 ± 0.8	119 ± 4/ 70 ± 4	464 ± 55	$2.5 \pm 3.2 \times 10^7$	$1.2 \pm 0.3 \times 10^6$	30.0 ± 1.4	
2913	F	4.7	6.0	110/50	731	3.20×10^6	2.75×10^5	23.1	PAH$^-$
3013	F	6.1	7.0	110/60	330	2.00×10^7	6.70×10^4	15.5	PAH$^-$
3113	F	6.7	5.0	100/75	886	3.60×10^8	1.17×10^7	20.6	PAH$^-$
3513	F	4.7	7.4	110/60	274	1.10×10^8	3.54×10^5	23.7	PAH$^-$
3613	F	4.7	7.0	110/70	312	1.40×10^7	2.68×10^6	21.4	PAH$^-$
6513	M	5.8	11.8	110/60	690	1.70×10^7	1.86×10^5	21.4	PAH$^-$
10413	M	5.8	8.8	110/75	397	1.20×10^8	1.17×10^7	21.0	PAH$^-$
10713	M	6.9	6.8	135/95	378	1.20×10^6	1.08×10^6	21.1	PAH$^-$
11313	M	5.8	8.0	140/80	679	1.00×10^7	2.19×10^2	23.0	PAH$^-$
11413	M	5.8	8.8	130/70	188	7.10×10^6	7.93×10^5	18.86	PAH$^-$
Mean ± SEM		5.7 ± 0.2	7.7 ± 0.6	117 ± 4/ 70 ± 4	487 ± 75	$6.6 \pm 3.5 \times 10^7$	$2.9 \pm 1.5 \times 10^6$	21.0 ± 0.7	

F, female; M, male

performed right heart catheterization on 21 (12 male, 9 female) healthy adult rhesus macaques (Table 1). The systemic blood pressures, right atrial pressure, right ventricular systolic pressure, and mPAP of normal rhesus macaques were within normal human ranges (Figure 2). All animals then were infected with SIV for longitudinal analysis of hemodynamic, virologic, and immunologic parameters (Table 1).

All SIV-infected macaques displayed the typical decline in peripheral blood $CD4^+$ T-cell numbers (mean chronic-phase $CD4^+$ T-cell count, 464.3 cells/μL) and a characteristic chronic-phase plasma viral level (mean RNA copies/mL, 2.02×10^6; Figure 3).

Association of SIV infection with early hemodynamic alterations. We previously reported a significant elevation in right heart and pulmonary arterial pressures in end-stage SIV- and SIV–HIV-infected macaques compared with naïve animals.[12] In the present study, we performed serial RHC and echocardiography before SIV infection and at 6 and 12 mo after SIV infection. Right atrial pressure, right ventricular systolic pressure, and mPAP were significantly elevated ($P < 0.05$) at 6 and 12 mo after infection compared with baseline values, whereas systemic blood pressure remained stable throughout the study (Figure 4). During the course of study, 11 of the 21 macaques had elevated mPAP greater than 25 mm Hg and were classified as PAH$^+$; the remaining 10 animals maintained normal pressure throughout SIV infection (PAH$^-$). PAH was defined as mPAP ≥ 25 mm Hg according to human PAH clinical criteria (Figure 2).

	Human	Rhesus macaque
Right atrial pressure	0–6	3.1 ± 0.3
Right ventricular systolic pressure	15–30	27.1 ± 1.2
Mean pulmonary artery pressure	9–19	15.4 ± 0.6
Systolic blood pressure	<120	119.8 ± 3.2
Diastolic blood pressure	<80	70.0 ± 2.3

Figure 2. Hemodynamics in humans and rhesus macaques (mm Hg; mean ± 1 SD; $n = 21$. Human reference values are from reference 21.

Phenotypic variation of the PAH progression in SIV-infected macaques. Longitudinal analyses revealed variations in the pattern of hemodynamic alterations in the macaques with elevated mPAP (PAH$^+$ animals). Of the 11 PAH$^+$ animals, 6 (54%) had evidence of progressive disease (P-PAH$^+$) in light of increased pressures at 6 and 12 mo after infection (Figure 4). In contrast, the remaining 5 macaques (45%) exhibited elevated pressures that peaked at 6 mo after infection (baseline mPAP, 16.6 mm Hg; 6 mo mPAP, 31.5 mm Hg; $P = 0.01$) and then declined at study termination (end mPAP, 20.34 mm Hg; $P = 0.29$ [compared with baseline]). These 5 animals were designated as having transient PAH (T-PAH$^+$) in further analyses.

Clinical correlates of hemodynamic parameters and PAH disease progression. We examined clinical parameters with elevated mPAP, right heart pressures, and disease outcomes (that is, progressive compared with transient PAH; Table 1). Variables

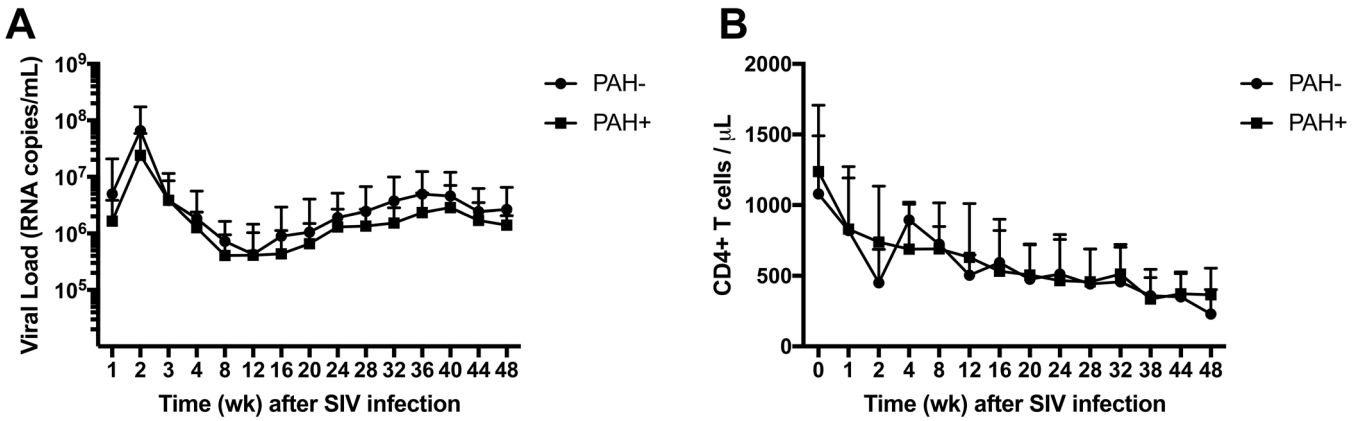

Figure 3. SIV plasma viral loads and CD4 T cell levels are similar in PAH$^+$ and PAH- SIV-infected rhesus macaques. Serial blood samples were collected throughout the study. (A) Mean plasma virus loads showed no significant difference between macaques that developed PAH (PAH$^+$, $n = 11$) and macaques that maintained normal hemodynamic parameters throughout the study (PAH$^-$, $n = 10$). (B) Peripheral blood CD4$^+$ T-cell levels in PAH$^+$ ($n = 11$) and PAH$^-$ ($n = 10$) macaques.

including sex, baseline weight and age, systemic blood pressure, peak viral load and set point, and CD4$^+$ T-cell counts at baseline or after SIV infection were not associated with either T-PAH$^+$ or P-PAH$^+$ or absolute pulmonary pressures in the PAH$^+$ versus PAH$^-$ groups.

Echocardiographic analysis of RV function in SIV-PAH$^+$ macaques. Compared with baseline values, neither cardiac index nor flow differed at 6 or 12 mo after infection, despite increases in systolic RV pressure. As a measure of ventricular performance, we evaluated the maximal rate of pressure rise during ventricular contraction (max dP/dt),[31] which was elevated compared with baseline values at 6 mo after infection in macaques with T-PAH$^+$ ($P = 0.002$) and at study end in P-PAH$^+$ animals ($P = 0.02$). When max dP/dt was normalized by using right ventricular systolic pressure (contractile index), there were no significant differences between groups at any time point, indicating early-stage PAH. Total pulmonary vascular resistance index (defined as mPAP/cardiac index) differed between groups at baseline, which can be attributed to variations in flow (cardiac index) given that mPAP was similar. Changes in the total pulmonary vascular resistance index over time paralleled changes in mPAP within groups but did not differ significantly between groups at 6 mo and terminal time points, reflecting variability in flow. During diastole, end-diastolic pressure was elevated at 6 mo after infection compared with baseline ($P = 0.005$) in T-PAH$^+$ animals. In P-PAH$^+$ macaques, minimum dP/dt decreased ($P = 0.02$) at termination compared with baseline, indicating a decrease in relaxation time as PAH progressed; this result corresponded to an increase in end-diastolic pressure in this group (Figure 5).

Evaluation of RV wall and myocyte hypertrophy in SIV-PAH macaques. RV wall thickness was evaluated by serial echocardiography in a subset of animals at baseline, 6 mo after infection and at study termination. RV wall thickness did not differ significantly between PAH$^+$ compared with PAH$^-$ animals ($n = 16$) at any time point (baseline, 0.41 ± 0.02 cm; 6 mo, 0.43 ± 0.02 cm) or at study termination (0.41 ± 0.02 cm).

At study termination, morphometric analysis of myocyte thickness revealed no significant difference ($P = 0.63$) between PAH$^+$ ($n = 11$; 26.43 ± 0.50 μm) and PAH$^-$ ($n = 10$; 26.12 ± 0.41 μm) animals.

Myocardial and lung fibrosis. We previously reported that SIV- and SHIV-infected macaques with hemodynamic evidence of PAH have an increased frequency of pulmonary arterial hyperplasia and increased periarteriolar fibrillary collagen content compared with non-PAH animals.[3,11] In the present study, we examined RV and LV tissue collagen deposition in PAH$^+$ and PAH- animals. Interestingly, RV collagen content was increased in SIV-infected animals at study termination ($n = 21$; 10 to 12mpi) compared with LV (Figure 6 A), however RV collagen deposition was significantly higher in PAH$^+$ compared with PAH- (Figure 6 B; $n = 11$; PAH$^+$ = 8.21% collagen/170 mm^2; PAH$^-$ =4.92% collagen/170 mm^2; $P = 0.01$).

PAH$^+$ macaques had significantly ($P < 0.0001$) more pulmonary periarteriolar collagen content than PAH$^-$ macaques (Figure 6 G), and P-PAH$^+$ animals more ($P < 0.0001$) than T-PAH$^+$ macaques (Figure 6 H). In addition, 2 PAH$^-$ macaques had higher levels of periarteriolar collagen content than the remaining 8 PAH$^-$ animals ($n = 9$: mean parallel, 9.4%; mean orthagonal, 6.86%; $n = 2$: mean parallel, 43.39%; mean orthagonal, 45.39%; $P \leq 0.0001$). These 2 animals also had elevated mPAP after SIV infection (23.07 and 23.7 mm Hg) compared with baseline values (13.3 and 14.4 mm Hg). Although these 2 macaques did not meet the cut-off mPAP values for PAH during the course of study, the increased collagen content and elevated pulmonary arterial pressures suggest that they were progressing toward PAH.

Relationship between increased RV glucose metabolism and SIV-PAH. Consistent with hemodynamic and histopathologic data suggesting RV alterations in SIV-PAH$^+$ monkeys, we observed changes in glucose uptake in the RV of SIV-PAH$^+$ macaques as assessed by ^{18}FDG-PET-CT (Figure 7). Standard ^{18}FDG uptake value (SUV) ratios of RV and LV were increased ($P = 0.02$) in SIV-infected, PAH$^+$ macaques ($n = 6$) at termination compared with baseline animals ($n = 10$), and there was a positive correlation ($P = 0.007$, $R^2 = 0.86$) between peak mPAP after SIV infection and RV:LV SUV ratio in PAH$^+$ macaques ($n = 6$). Figure 7 shows prominent RV FDG uptake in an SIV-PAH$^+$ macaque (Figure 7 C and E) compared with an uninfected animal (Figure 7 D).

Correlation between pulmonary inflammation and SIV-PAH. Because there is considerable evidence that inflammatory processes contribute to PAH development and severity,[10] we evaluated the relationship between PAH status and inflammatory mediators in plasma and BALF (Figure 1) throughout SIV infection.

Independent of their PAH status, all SIV-infected macaques demonstrated increases ($P = 0.05$) in plasma IL6, monocyte

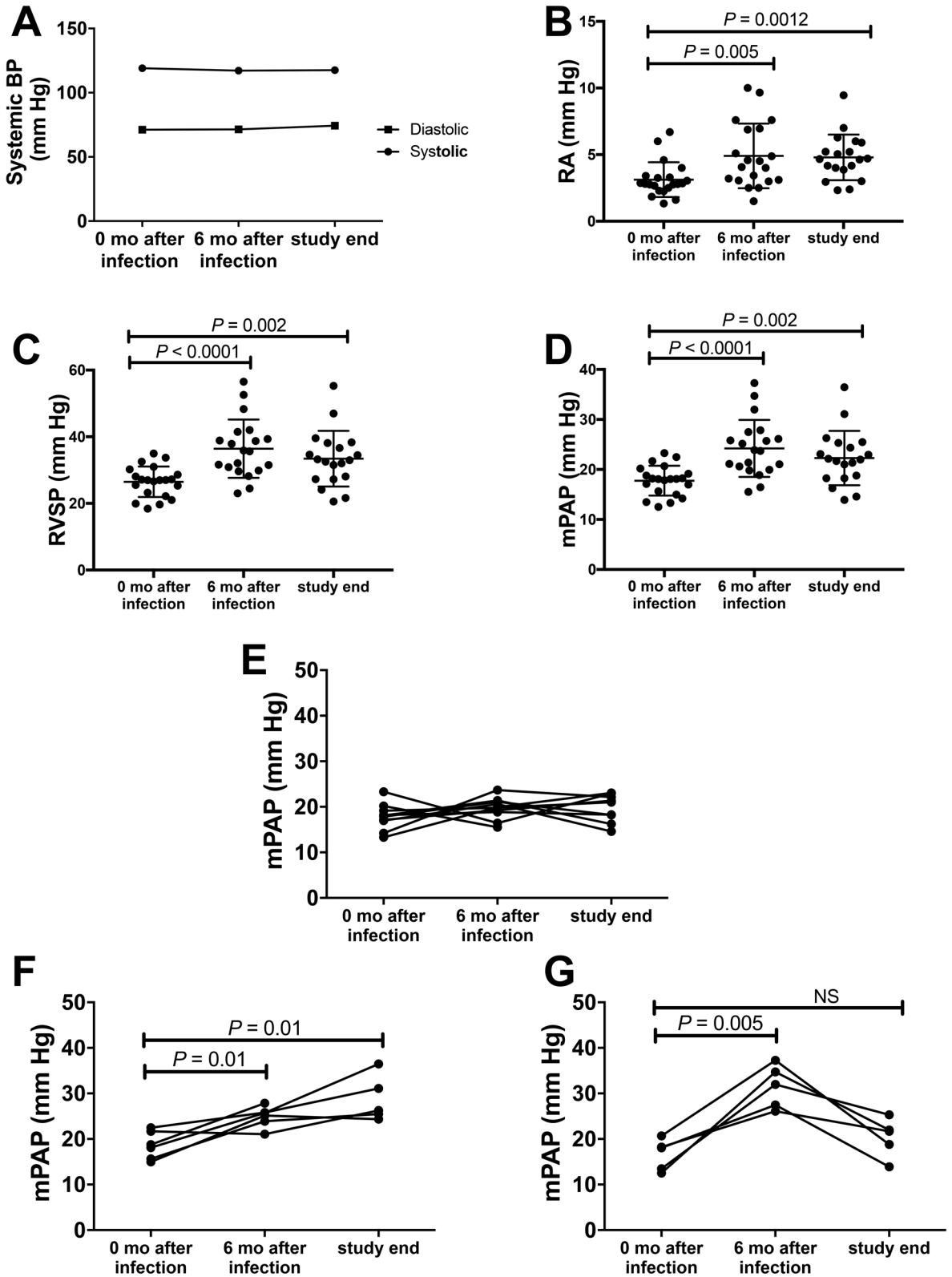

Figure 4. SIV infection of rhesus macaques is associated with increased right atrial (RA), right ventricular (RV), and mean pulmonary arterial pressures (mPAP) by 6 mo after infection. Systemic blood pressure measurements and right heart catheterization were performed on adult rhesus macaques at baseline (0 mo after infection), 6 mo after infection, and at study end (10–12 mo after SIV infection. (A) Mean systemic systolic and diastolic pressures remained in the normal range throughout SIV infection. (B) Right RA, (C) RV systolic pressure (RVSP), and (D) mean pulmonary artery pressure (mPAP) were significantly increased at 6 mo after infection and at study end. (E) A subset of SIV-infected macaques maintained mPAP in the normal range until 12 mo after infection (PAH^-; $n = 10$). (F) Macaques with progressive PAH^+ (P-PAH^+) had significant elevation of mPAP at 6 mo after infection ($n = 6$) and at study end compared with baseline. (G) Macaques with transient PAH^+ (T-PAH^+) had a significant increase in mPAP at 6 mo after infection compared with baseline but decreased values by the terminal time point that did not return to baseline ($P = 0.29$).

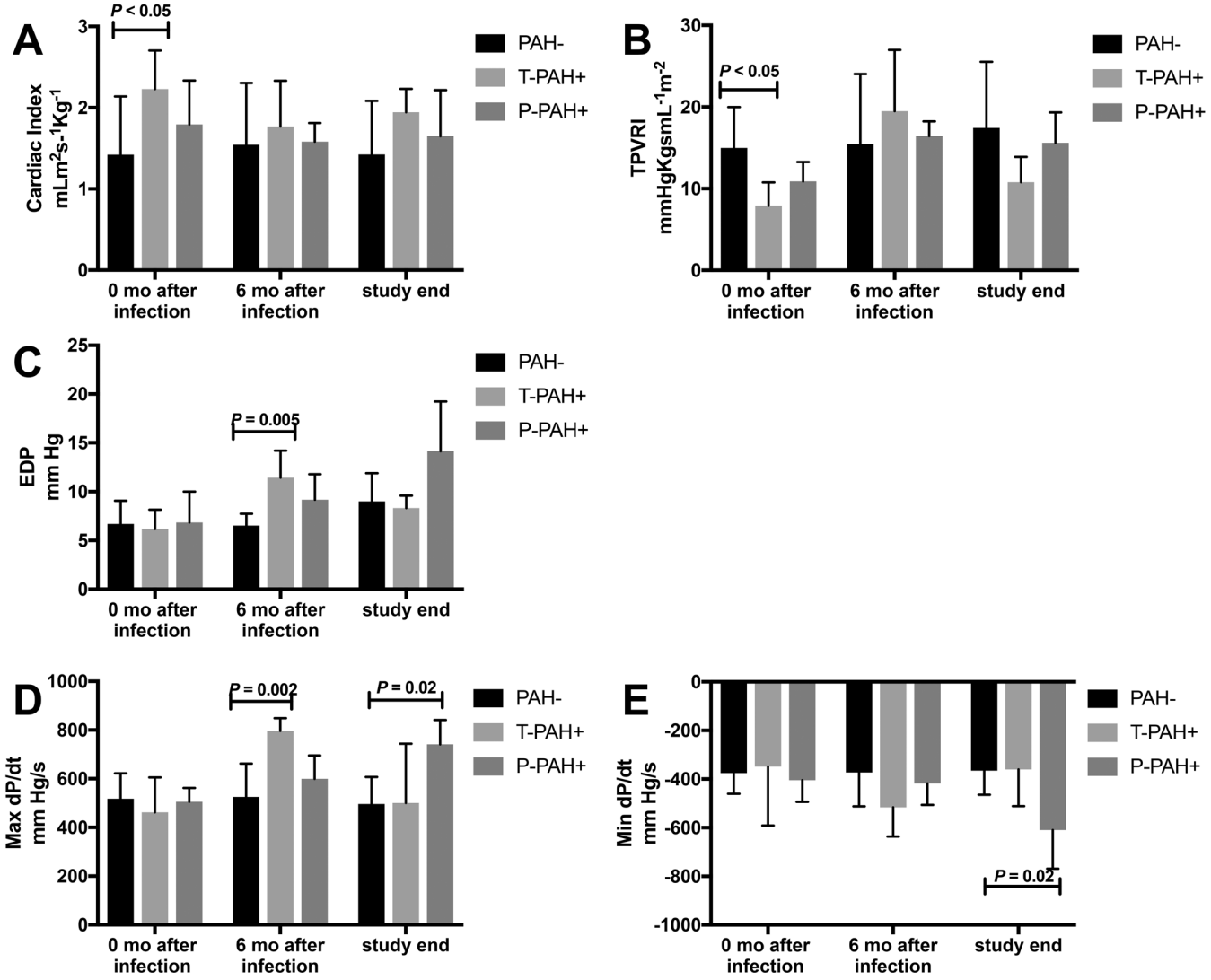

Figure 5. Echocardiographic analysis of RV function. (A) Neither cardiac index nor flow at 6 mo after infection or study end differed from baseline measures despite early increases in RV pressure. (B) Total pulmonary vascular resistance index (TPVRI) had no significant differences between groups at 6mo after infection or at study end. (C) End-diastolic pressure (EDP) in T-PAH$^+$ macaques was elevated at 6 mo after infection compared with baseline. (D) In macaques with T-PAH$^+$, maximal dP/dt was elevated at 6 mo after infection compared with baseline; in the P-PAH$^+$ group, maximal dP/dt was elevated at study end. (E) Minimal dP/dt in P-PAH$^+$ animals was decreased at study end compared with baseline.

chemoattractant protein 1/C-C motif chemokine ligand (CCL) 2, macrophage-derived chemokine/CCL22, IFN-inducible T-cell α chemoattractant/C-C-C motif chemokine ligand (CXCL) 11, VEGF, IFNγ-inducible protein (IP) 10/CXCL10, C-reactive protein, and TNFα compared with baseline levels (Table 2). Plasma IL10 levels were decreased at study termination. BALF samples had increased levels of RANTES/CCL5, IL17, eotaxin/CCL11, MIP1β/CCL4, IFN-inducible T-cell α chemoattractant/CXCL11, IP10/CXCL10, MIG/CXCL9 and macrophage-derived chemokine/CCL22 (Table 3).

At 6 mo after infection, plasma levels of IL15 were decreased ($P = 0.01$; Figure 8 A) in PAH$^+$ compared with PAH$^-$ macaques, and IL15 and mPAP were negatively correlated ($P = 0.01$; Figure 8 B). In BALF, TGFβ levels were increased ($P = 0.02$; Figure 8 C) in PAH$^+$ compared with PAH$^-$ animals and trended toward a significant correlation with mPAP ($P = 0.12$; Figure 8 D). At study termination, plasma levels of MIPα ($P = 0.02$; Figure 8 E) and TNFα were increased ($P = 0.05$; Figure 8 F) in PAH$^+$ compared with PAH$^-$ animals.

Discussion

We evaluated the development of SIV-associated PAH in rhesus macaques, as a model of HIV-PAH, by longitudinal analyses of hemodynamics, clinical parameters, and inflammatory mediators throughout disease progression. The ability to perform serial measurements of right heart and pulmonary pressures in this model greatly expands the ability to track early events in PAH pathogenesis, the progression of disease, clinical parameters, and biomarkers associated with disease susceptibility and responses to therapy. The most striking finding of the present study is the development of 3 distinct clinical outcomes of SIV infection with regard to hemodynamic changes. We found increased pulmonary and right heart pressures in a subgroup of macaques (11 of 21, 52%) after SIV infection. These animals were further characterized as having progressive PAH (6 of 21, 28.5%) or transient PAH (5 of 21; 23.8%) according to either further increases in pulmonary arterial and right heart pressures at 12 mo after infection or a return to near-preinfection levels, respectively. Despite the relatively early stage of PAH

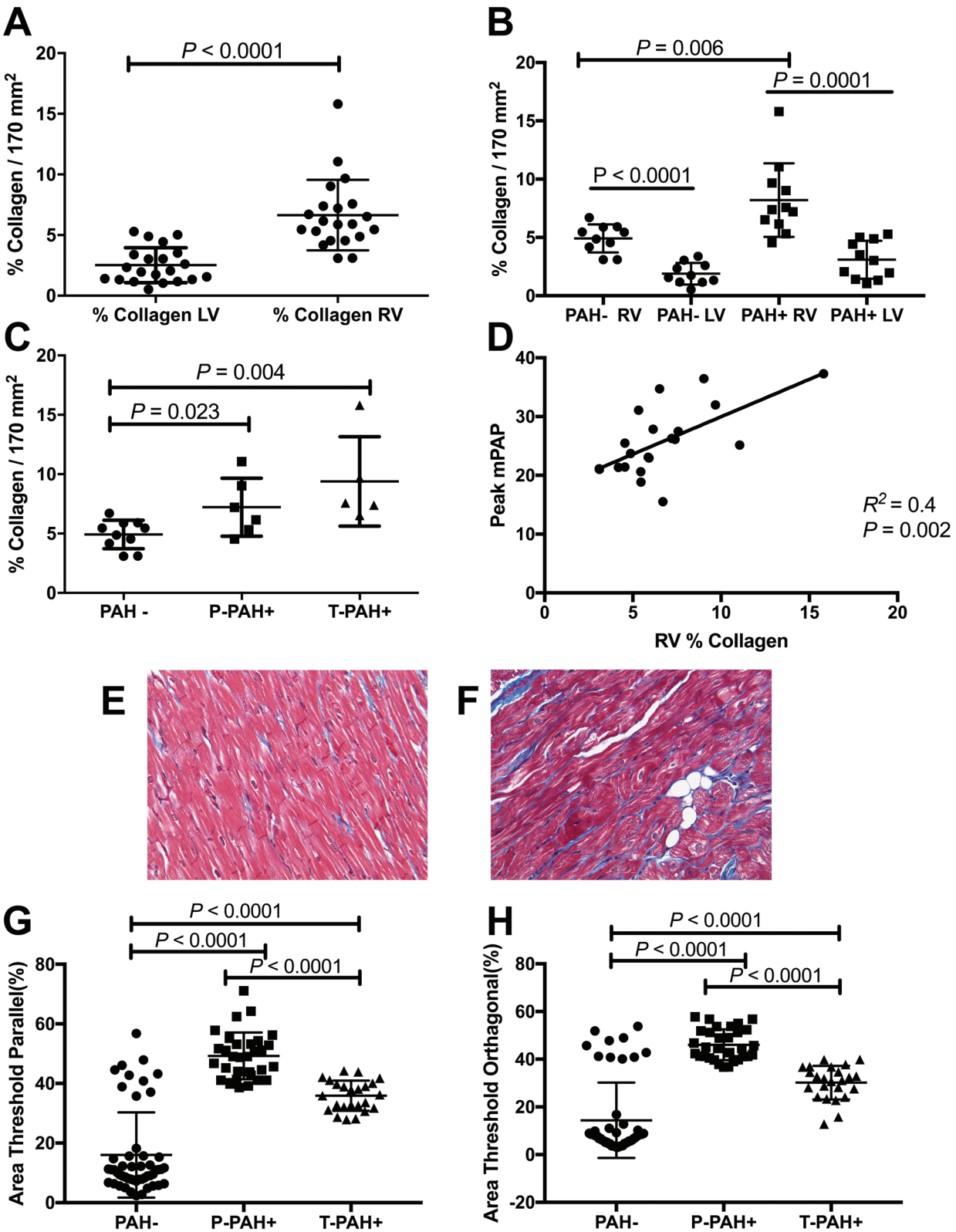

Figure 6. Relationship of collagen deposition and PAH status in SIV-infected macaques. (A) Collagen deposition was increased in the RV compared with the LV of SIV-infected macaques ($n = 21$). (B) When analyzed according to PAH status, RV collagen was significantly increased compared with LV in both the PAH$^+$ and PAH$^-$ animals, and RV collagen deposition was significantly higher in PAH$^+$ macaques ($n = 11$) compared with PAH$^-$ animals. (C) Collagen deposition was significantly elevated in P-PAH$^+$ ($n = 6$) and T-PAH$^+$ ($n = 5$) phenotypes compared with PAH$^-$ ($n = 10$). (D) Relationship of RV collagen deposition and peak pulmonary pressures in SIV-infected macaques ($n = 21$). (E and F) Representative images of RV from (E) PAH$^-$ and (F) PAH$^+$ animals. Trichrome stain; magnification, 40×. (G and H) PAH$^+$ macaques had significantly increased pulmonary periarteriolar collagen content compared with PAH- macaques. In both parallel and orthagonal evaluation, P-PAH$^+$ animals had significantly higher levels of periarteriolar collagen deposition than T-PAH$^+$ macaques.

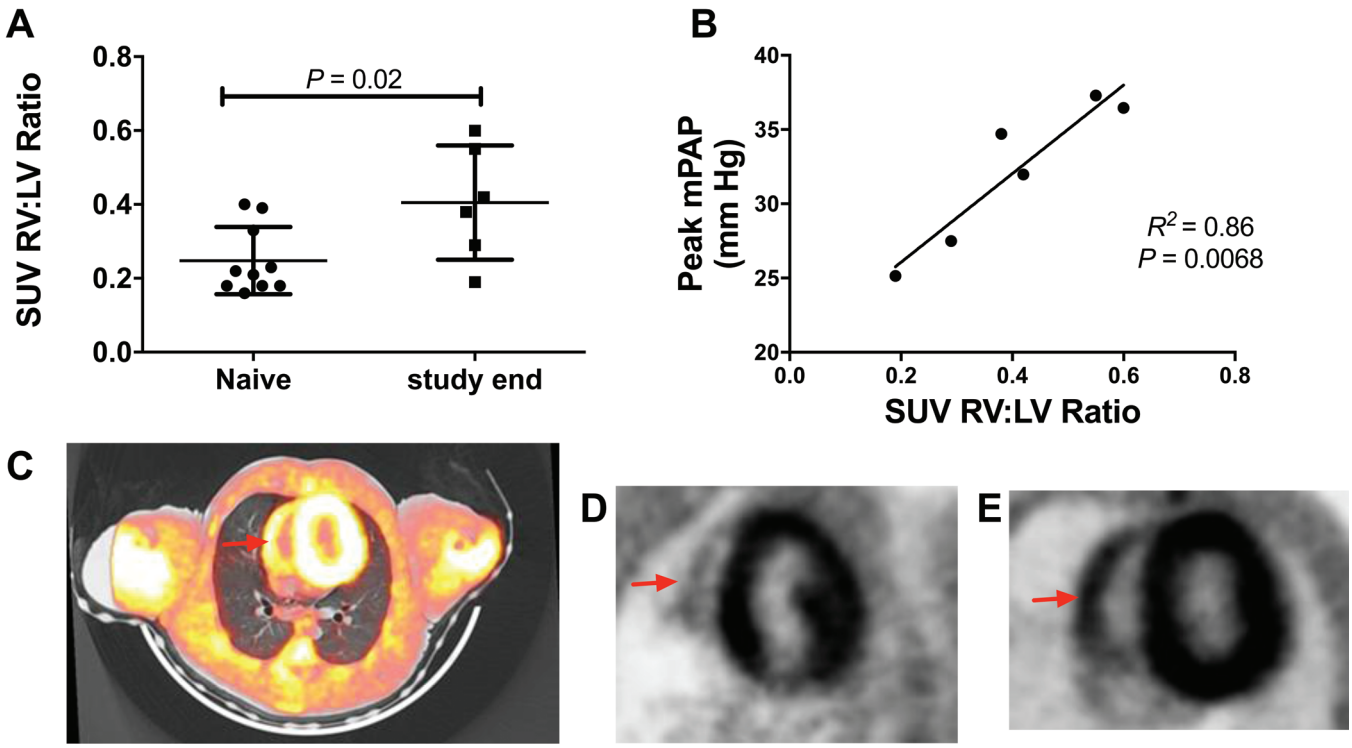

Figure 7. Fasting ^{18}F-fluorodeoxyglucose positron emission tomography coupled with CT (FDG-PET–CT) imaging of normal and SIV-infected macaques as a modality for assessing right heart glucose uptake. (A) At study end, SIV-infected macaques (n = 6) had higher RV:LV standard uptake value ratios (RV:LV SUV) compared with uninfected macaques (n = 10). (B) Relationship of peak mPAP and RV:LV SUV in PAH$^+$ macaques (n = 6). (C) Representative image of FDG-PET–CT overlay in a PAH$^+$ animal (red arrow, RV). (D and E) Representative PET images of a (D) PAH$^-$ macaque (red arrow, RV) and (E) PAH$^+$ animal.

Table 2. Serial analysis of plasma cytokines and chemokines

Cytokine or chemokine	Baseline	6 mo after SIV infection	P (baseline vs 6 mo)	12 mo after SIV infection	P (basleine vs 12 mo)
IL6	0.55 ± 0.33	1.33 ± 1.67	0.01	1.70 ± 1.83	0.0003
MCP1/CCL2	124.80 ± 60.86	167.43 ± 81.90	0.05	256.87 ± 278.88	0.0002
MDC/CCL22	246.53 ± 179.27	235.35 ± 167.42	0.86	341.33 ± 198.82	0.03
ITAC/CXCL11	5.93 ± 7.84	16.15 ± 15.05	0.02	23.14 ± 29.15	0.003
VEGF	0.17 ± 0.09	0.26 ± 0.21	0.04	0.24 ± 0.10	0.01
IP10/CXCL10	3.75 ± 2.64	5.17 ± 3.87	0.04	7.83 ± 7.57	0.02
IL10	1.59 ± 2.16	0.83 ± 0.68	0.2	0.88 ± 1.24	0.05
TNFα	5.51 ± 8.10	10.82 ± 23.17	0.49	10.69 ± 16.82	0.05
C-reactive protein[a]	5343 ± 2578	7601 ± 10826	0.81	27117 ± 33016	0.03
MIP1α/CCL3[b]	12.80 ± 9.69	16.15 ± 7.67	0.17	11.57 ± 7.85	0.76

CCL, C-C motif chemokine ligand; CXCL, C-X-C motif chemokine ligand; MCP, monocyte chemoattractant protein; MDC, macrophage-derived chemokine; MIP, macrophage inflammatory protein; CRP, C-reactive protein; IP, IFN-γ-inducible protein; ITAC, interferon-inducible T-cell α chemoattractant; VEGF, vascular endothelial growth factor
Data are given as mean ± 1 SD (pg/mL)
[a]Values at 6 and 12 mo differ significantly (P = 0.02).
[b]Values at 6 and 12 mo differ significantly (P = 0.01).

in these animals, RV dysfunction after SIV infection was evident, reflected in elevated RA and RV pressures measures by RHC, serial echocardiographic analyses, increased RV interstitial fibrosis, and PET-CT imaging, which revealed increased RV glucose uptake associated with increased mPAP. Although we found no evidence of RV hypertrophy on the basis of myocyte thickness, echocardiographic evaluation, or direct measurement of RV wall thickness postmortem, PAH$^+$ macaques had elevated RV collagen levels compared with PAH$^-$ animals. Interestingly, RV collagen content was elevated compared with LV in all SIV$^+$ monkeys, but RV collagen deposition in PAH$^+$ animals was greater than in the RV of PAH$^-$ animals. As expected, several inflammatory mediators were elevated in plasma and BAL fluid during SIV infection. We determined that although all SIV-infected animals had expected increases in several proinflammatory mediators throughout infection, only the plasma levels of MIP1α and TNFα and BALF level of TGFβ were significantly increased in PAH$^+$ animals compared with PAH$^-$ macaques. Interestingly, we noted decreased levels of plasma IL15 in PAH$^+$ animals and an inverse correlation with mPAP.

Table 3. Serial analysis of BALF cytokines and chemokines

Cytokine or chemokine	Baseline	6 mo after SIV infection	*P* (baseline vs 6 mo)	12 mo after SIV infection	*P* (baseline vs 12 mo)
RANTES/CCL5	15.34 ± 14.42	37.85 ± 43.14	0.06	99.38 ± 152.21	0.001
IL17	0.31 ± 0.63	2.63 ± 7.23	0.09	3.79 ± 4.81	0.001
MIP1β/CCL4	21.06 ± 35.11	54.54 ± 73.84	0.12	97.77 ± 156.47	0.02
ITAC/CXCL11[a]	19.40 ± 17.36	137.36 ± 282.28	0.01	367.11 ± 531.43	<0.0001
IP10/CXCL10	2.12 ± 2.21	27.00 ± 52.65	0.01	53.26 ± 65.66	<0.0001
Eotaxin/CCL11	1.08 ± 1.59	1.71 ± 1.95	0.17	10.81 ± 31.29	0.01
MDC/CCL22	187.03 ± 206.08	349.02 ± 529.90	0.22	702.75 ± 1932.83	0.02
MIG/CXCL9	0.69 ± 2.19	41.59 ± 104.21	0.08	296.62 ± 575.45	0.03

CCL, C-C motif chemokine ligand; CXCL, C-X-C motif chemokine ligand; IP, IFN-γ-inducible protein; ITAC, IFN-inducible T-cell α chemoattractant; MDC, macrophage-derived chemokine; MIG, monokine induced by IFNγ; MIP, macrophage inflammatory protein; RANTES, regulated on activation, normal T-cell expressed and secreted
Data are given as mean ± 1 SD (pg/mL)
[a]Values at 6 and 12 mo differ significantly ($P = 0.01$).

Despite the fact that antiretroviral therapy has transformed HIV infection from a predominantly immunosuppressive disease to a chronic disease state, PAH nevertheless remains a severe complication, and the prevalence of HIV-associated PAH has remained relatively steady in the antiretroviral therapy era. The prevalence of PAH during HIV infection has been estimated at 0.4% to 7%, although echocardiographic studies have reported higher prevalence of elevated pulmonary artery systolic pressure greater than 30 mm Hg, 35% to 66%; greater than 40 mm Hg6, 6% to 15.5% > 40 mm Hg) in HIV-infected than in HIV-noninfected men and women.[16,24,25,35,36] The high prevalence of elevated pulmonary arterial and right-heart pressures in SIV-infected macaques (50%) compared with HIV–PAH, as measured by RHC, may reflect an early, transient process in experimental infections that also occur in HIV$^+$ persons prior to development of clinical symptoms.

Due to the prospective design of this study, we were able to capture 3 distinct phenotypes with regard to hemodynamic profiles that were not directly associated with SIV disease severity. The observation of a transient phenotype in SIV-associated PAH suggests that early hemodynamic changes occur, but these responses may be reversible at this relatively early stage of disease. Several experimental studies of PAH and clinical trials of therapeutic interventions have demonstrated that PAH can be reversed under circumstances and mechanisms that are not fully understood.[4,7,33] Whether reversal of remodeled vasculature is limited to specific types of PAH or whether there is a 'tipping point' in disease progression after which reversal is not achievable is unknown, and the SIV-PAH model may be particularly useful in further interrogating this process.

Assessment of the relationship of PAH to HIV infection-related parameters has produced conflicting results.[4,7,8] HIV-related PAH is diagnosed at all stages of infection, and consensus has not yet been achieved regarding the relationship among CD4$^+$ T-cell counts, viral load, and PAH.[39,22] In the absence of potential confounding parameters of HIV-PAH studies, such as antiretroviral use, preexisting lung disease, cigarette smoking, and intravenous drug use, our studies show that SIV infection alone induces PAH in a subset of animals. Although several studies have reported in vitro evidence of a role for HIV proteins in the pathogenesis of pulmonary vascular injury and PAH,[29] we did not find a correlation between hemodynamic parameters and peak viral load, viral set points or plasma CD4 T cell nadir in the current study. These findings do not exclude the possibility that specific viral proteins play roles in pathogenesis; however the lack of an association between viral load and the incidence or severity of SIV-PAH (and during HIV infection) supports the hypothesis that secondary factors such as host-specific responses to viral infection or genetic factors may alter the disease progression.

Pulmonary vascular remodeling and vascular stiffness are important pathologic features that contribute to pulmonary vascular resistance and increase pulmonary arterial pressure in PAH. Our laboratory and others have noted previously that SIV-infected macaques exhibit pulmonary vascular remodeling and pruning consistent with PAH, although the extent of remodeling is relatively mild compared with human PAH.[5,11,12,19] The current study extends the observation of fibrotic processes to include the RV, suggesting that increased RV fibrosis is a relatively early manifestation of SIV-PAH and occurs in advance of significant pulmonary vascular remodeling. Although we observed increased RA and RV pressures associated with increased RV collagen deposition in PAH$^+$ animals, we did not find convincing evidence of myocyte hypertrophy or overt RV wall thickening, suggesting that the early manifestation of RV involvement is associated with a predominant fibrotic process and possibly metabolic alterations.

Metabolic changes in PAH pulmonary arteries and RV have been shown to occur in humans and in experimental rodent models.[1,26,20,37] To further explore RV involvement in disease progression, we evaluated metabolic changes using a novel FDG PET–CT imaging arrangement for primate cardiac assessment. The RV wall was clearly identifiable by PET–CT and we demonstrated that FDG RV:LV SUV ratio was significantly increased in SIV-PAH macaques at 12 mo after SIV infection compared with preinfection values. It is interesting that although several other experimental animal studies have shown similar metabolic alterations in hypertrophied RV myocardium due to long-term RV overload, we found little evidence of frank myocardial hypertrophy associated with increased RV glucose uptake in this model. We were unable to perform serial PET scans to follow disease progression, but the results regarding RV glucose uptake are consistent with the clinical observations that during PAH, the right heart has pathologic glycolytic metabolism that is related to cardiac dysfunction. These results suggest that metabolic imaging in an NHP model may be a useful means of assessing and predicting disease progression and monitoring experimental therapeutic interventions.

Chronic inflammatory responses associated with HIV infection have been implicated as a driving force in the development of HIV-associated diseases, including PAH.[4,6] Furthermore, it has long been recognized that aberrant immune reactivity

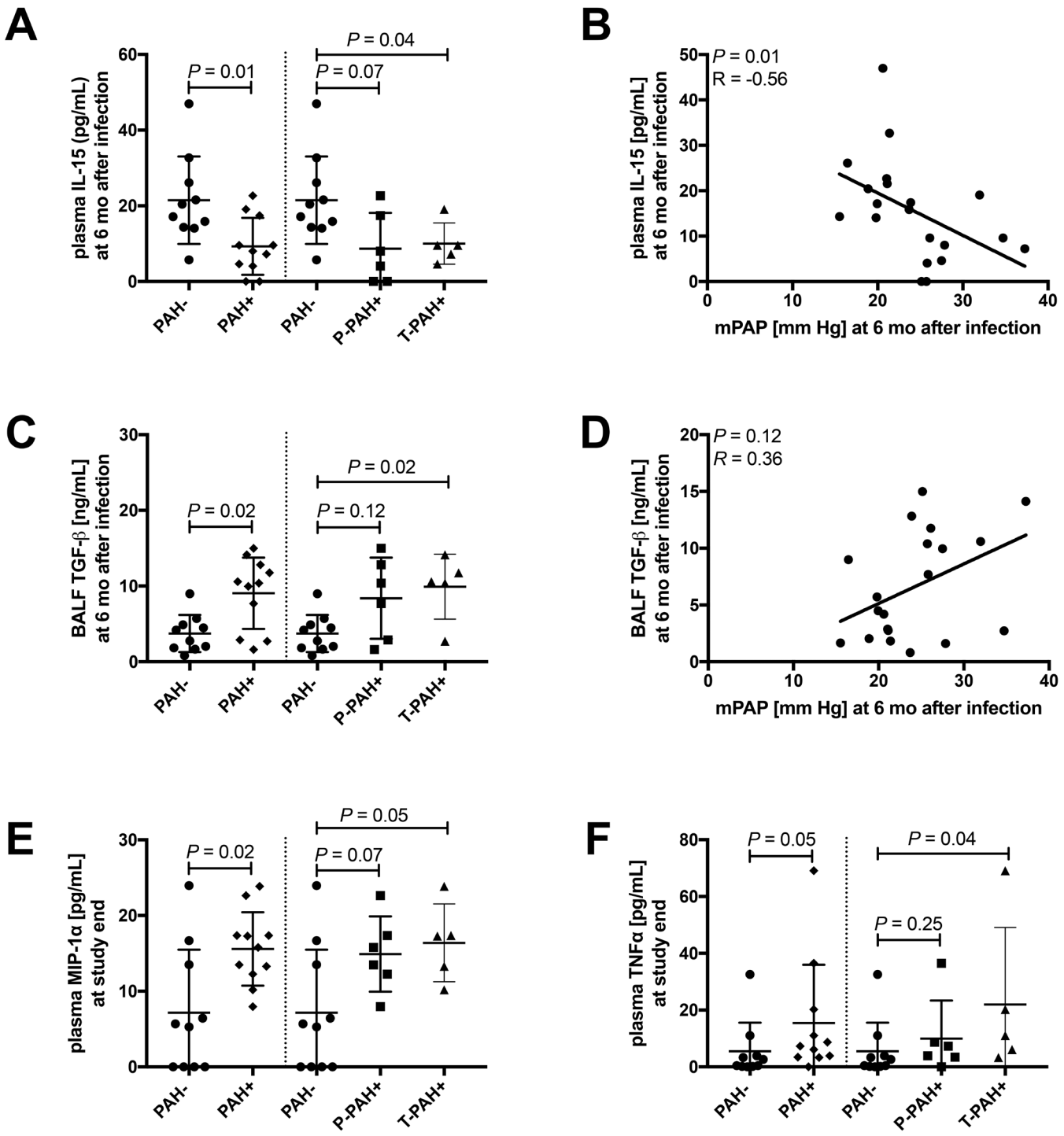

Figure 8. Compared with PAH⁻ animals, macaques developing PAH⁺ showed higher baseline plasma levels of chemokines involved in monocyte–macrophage trafficking and elevated levels of growth factor TGFβ in BALF at 6 mo after infection. We quantified a total of 31 cytokines, chemokines, and growth factors in serial plasma and BALF samples. Differences in inflammatory markers between PAH⁺ and PAH⁻macaques at 6 mo after infection and at study end were assessed by using Mann–Whitney tests. To test for associations between mPAP and each immune marker, Spearman correlation was used. All graphs of correlation analysis, show regression lines.(A) At 6 mo after infection, plasma levels of IL15 were decreased ($P = 0.01$) in PAH⁺ compared with PAH⁻ macaques, and (B) IL15 and mPAP were negatively correlated ($P = 0.01$). In BALF, (C) TGFβ levels were increased ($P = 0.02$; Figure 8 C) in PAH⁺ compared with PAH⁻ animals and (D) trended toward a significant correlation with mPAP ($P = 0.12$). At study termination, plasma levels of (E) MIPα ($P = 0.02$) and (F) TNFα were increased ($P = 0.2$ and $P = 0.05$, respectively) in PAH⁺ compared with PAH⁻ animals.

and inflammation are hallmarks of PAH and that activation and tissue infiltration by various inflammatory mediators likely influences pulmonary vascular remodeling and vascular stiffness.[9,10,16,28] In the serial evaluation of plasma and BALF cytokines and chemokines associated with inflammation, we found—as expected—increased levels of key mediators (including IL6 and TNFα [Figure 1]), during the course of SIV infection compared with baseline values. Regarding PAH phenotypes, we found increased levels of plasma MIP1α and TNFα (at 12 mo after infection) and increased TGFβ (at 6 mo after infection) in the

BALF of PAH$^+$ animals compared with PAH$^-$ macaques. Both MIP1α and TNFα are elevated in human PAH, and both factors are activated by the HIV protein negative factor (Nef).[2,23,27] MIP1α, a macrophage-derived inflammatory protein has been shown to induce secretion of TNFα, IL1, and IL6 and thus the detection of MIP1α in PAH$^+$ animals suggests that this cytokine may have an important role in the development of the subsequent inflammatory responses of PAH by contributing to the recruitment of mononuclear cells and modulating the production of downstream cytokines including TNFα and IL6. These findings illustrate an important feature of our SIV-PAH macaque model as a useful system for the interrogation of the chronology of events associated with immune-mediated pathology of PAH.

Interestingly, plasma IL15 concentrations were elevated in PAH$^-$compared with PAH$^+$ macaques and inversely related to mPAP. This inverse relationship with disease phenotype and pulmonary pressure is somewhat counterintuitive, given that IL15 functions as a danger signal to regulate tissue-resident T cells and inhibit T regulatory cell expansion. Experimental overexpression of IL15 is also associated with increased tissue destruction.[15] IL15 has a wide tissue distribution and is expressed by several cell types including hematopoietic (for example, T and B cells, monocytes, macrophages) and nonhematopoietic cells (for example, endothelial, pulmonary epithelial cells)—all of which cells are thought to play key roles in PAH pathogenesis.[15] IL15 is an immunologic 'first responder' that is critical for relaying signals of tissue distress and is central to the regulation of CD8$^+$ T cell in the peripheral blood and tissue resident cells.[15] IL15 receptors have recently been identified on mice cardiomyocytes and supplemental IL15 has been shown to mediate protection against cell death under hypoxic condition in vitro.[40] This protective role of IL15 in nonhematopoietic cells and our observation of decreased circulating IL15 in the plasma of SIV-PAH$^+$ macaques may point to a novel role for IL15. In addition, decreasing levels of IL15 may be involved in the development of myocardial metabolic alterations observed in PAH.[40] Further insight regarding the mechanism by which IL15 influences cellular responses in the context of PAH will be found by an examination of local pulmonary and cardiac tissue expression and the characterization of local cells that may be receiving IL15-mediated signals. Immunologic evaluation of the lung and cardiac tissue of PAH$^+$ and PAH$^-$ animals used in this study is ongoing.

This study has several limitations. First, because of the few animals in each group, we may not have had sufficient power to detect significant differences in some of the inflammatory parameters measured. However, we have recently observed noteworthy phenotypic differences and activation states of monocytes and macrophages in SIV-infected animals that developed PAH compared with PAH$^-$ animals.[34] In addition, there are limitations regarding noninvasive estimates of flow as well as estimating of mPAP from right ventricular systolic pressure. As is the case in the diagnosis of human PAH, the we based the determination of PAH in this study on findings from RHC, and noninvasive echocardiography parameters were used to supplement the characterization. In animals in which direct pulmonary arterial pressure was not obtained by RHC, we estimated pulmonary pressures based on right ventricular systolic pressure[38] and validated this method in rhesus macaques, as described earlier.

PAH continues to be a severe complication of HIV infection. The SIV-PAH macaque model we report here provides a means for investigating the pathogenesis of HIV-PAH in a highly relevant animal model and shows for the first time that the progression of PAH may take a variable course that is not directly associated with severity of viral infection, CD4$^+$ T-cell–related immunosuppression or general chronic inflammation. Although secondary insults—such as illicit drug use, underlying pulmonary disease, and antiretroviral therapy—may contribute to or worsen symptoms, the present study demonstrates that viral infection alone is sufficient to produce hemodynamic derangement and tissue pathology associated with PAH. The SIV-PAH macaque model will help define the order of specific inflammatory events elicited during early stages of disease progression, particularly at time points when disease reversal may be possible. These studies will provide insight into specific pathways that may serve as therapeutic targets for the development of new, specific treatment options for PAH.

Acknowledgments

We thank Dr Christopher Janssen and Michael Bennett Johnston for veterinary support and Dr Michael Murphey-Corb for providing SIV virus stocks and titration information.

This work was supported by NIH grants P01 HL121095, R56 HL125276, R01 HL131449, and R01 HL138437; the Georgia Research Alliance; and the University of Georgia Research Foundation.

References

1. **Archer SL, Fang YH, Ryan JJ, Piao L.** 2013. Metabolism and bioenergetics in the right ventricle and pulmonary vasculature in pulmonary hypertension. Pulm Circ **3:**144–152. https://doi.org/10.4103/2045-8932.109960.
2. **Arcot SS, Lipke DW, Gillespie MN, Olson JW.** 1993. Alterations of growth factor transcripts in rat lungs during development of monocrotaline-induced pulmonary hypertension. Biochem Pharmacol **46:**1086–1091. https://doi.org/10.1016/0006-2952(93)90675-M.
3. **Bertero T, Oldham WM, Cottrill KA, Pisano S, Vanderpool RR, Yu Q, Zhao J, Tai Y, Tang Y, Zhang YY, Rehman S, Sugahara M, Qi Z, Gorcsan J 3rd, Vargas SO, Saggar R, Saggar R, Wallace WD, Ross DJ, Haley KJ, Waxman AB, Parikh VN, De Marco T, Hsue PY, Morris A, Simon MA, Norris KA, Gaggioli C, Loscalzo J, Fessel J, Chan SY.** 2016. Vascular stiffness mechanoactivates YAP/TAZ-dependent glutaminolysis to drive pulmonary hypertension. J Clin Invest **126:**3313–3335. https://doi.org/10.1172/JCI86387.
4. **Butrous G.** 2015. Human immunodeficiency virus-associated pulmonary arterial hypertension: considerations for pulmonary vascular diseases in the developing world. Circulation **131:**1361–1370. https://doi.org/10.1161/CIRCULATIONAHA.114.006978.
5. **Chalifoux LV, Simon MA, Pauley DR, MacKey JJ, Wyand MS, Ringler DJ.** 1992. Arteriopathy in macaques infected with simian immunodeficiency virus. Lab Invest **67:**338–349.
6. **Deeks SG.** 2011. HIV infection, inflammation, immunosenescence, and aging. Annu Rev Med **62:**141–155. https://doi.org/10.1146/annurev-med-042909-093756.
7. **Degano B, Guillaume M, Savale L, Montani D, Jais X, Yaici A, Le Pavec J, Humbert M, Simonneau G, Sitbon O.** 2010. HIV-associated pulmonary arterial hypertension: survival and prognostic factors in the modern therapeutic era. AIDS **24:**67–75. https://doi.org/10.1097/QAD.0b013e328331c65e.
8. **Degano B, Sitbon O, Simonneau G.** 2009. Pulmonary arterial hypertension and HIV infection. Semin Respir Crit Care Med **30:**440–447. https://doi.org/10.1055/s-0029-1233313.
9. **Dorfmüller P, Perros F, Balabanian K, Humbert M.** 2003. Inflammation in pulmonary arterial hypertension. Eur Respir J **22:**358–363. https://doi.org/10.1183/09031936.03.00038903.
10. **El Chami H, Hassoun PM.** 2012. Immune and inflammatory mechanisms in pulmonary arterial hypertension. Prog Cardiovasc Dis **55:**218–228. https://doi.org/10.1016/j.pcad.2012.07.006.
11. **George MP, Brower A, Kling H, Shipley T, Kristoff J, Reinhart TA, Murphey-Corb M, Gladwin MT, Champion HC, Morris A, Norris KA.** 2011. Pulmonary vascular lesions are common in SIV- and SHIV-env-infected macaques. AIDS Res Hum Retroviruses **27:**103–111. https://doi.org/10.1089/aid.2009.0297.

12. **George MP, Champion HC, Simon M, Guyach S, Tarantelli R, Kling HM, Brower A, Janssen C, Murphy J, Carney JP, Morris A, Gladwin MT, Norris KA.** 2013. Physiologic changes in a nonhuman primate model of HIV-associated pulmonary arterial hypertension. Am J Respir Cell Mol Biol **48:**374–381. https://doi.org/10.1165/rcmb.2011-0434OC.
13. **Hsue PY, Deeks SG, Farah HH, Palav S, Ahmed SY, Schnell A, Ellman AB, Huang L, Dollard SC, Martin JN.** 2008. Role of HIV and human herpesvirus 8 infection in pulmonary arterial hypertension. AIDS **22:**825–833. https://doi.org/10.1097/QAD.0b013e3282f7cd42.
14. **Institute for Laboratory Animal Research.** 2011. Guide for the care and use of laboratory animals, 8th ed. Washington (DC): National Academies Press.
15. **Jabri B, Abadie V.** 2015. IL15 functions as a danger signal to regulate tissue-resident T cells and tissue destruction. Nat Rev Immunol **15:**771–783. https://doi.org/10.1038/nri3919.
16. **Lammers S, Scott D, Hunter K, Tan W, Shandas R, Stenmark KR**.2012. Mechanics and function of the pulmonary vasculature: implications for pulmonary vascular disease and right ventricular function. Compr Physiol 2:295–319. https://doi.org/10.1002/cphy.c100070.
17. **Kherbeck N, Tamby MC, Bussone G, Dib H, Perros F, Humbert M, Mouthon L.** 2011. The role of inflammation and autoimmunity in the pathophysiology of pulmonary arterial hypertension. Clin Rev Allergy Immunol **44:**31–38. https://doi.org/10.1007/s12016-011-8265-z.
18. **Marecki J, Cool C, Voelkel N, Luciw P, Flores S.** 2005. Evidence for vascular remodeling in the lungs of macaques infected with simian immunodeficiency virus–HIV NEF recombinant virus. Chest **128 6 Suppl:**621S–622S. https://doi.org/10.1378/chest.128.6_suppl.621S.
19. **Marecki JC, Cool CD, Parr JE, Beckey VE, Luciw PA, Tarantal AF, Carville A, Shannon RP, Cota-Gomez A, Tuder RM, Voelkel NF, Flores SC.** 2006. HIV1 Nef is associated with complex pulmonary vascular lesions in SHIV–Nef-infected macaques. Am J Respir Crit Care Med **174:**437–445. https://doi.org/10.1164/rccm.200601-005OC.
20. **Marsboom G, Wietholt C, Haney C, Toth PT, Ryan JJ, Morrow E, Thenappan T, Bache-Wiig P, Piao L, Paul J, Chen CT, Archer SL.** 2012. Lung ^{18}F-fluorodeoxyglucose positron emission tomography for diagnosis and monitoring of pulmonary arterial hypertension. Am J Respir Crit Care Med **185:**670–679. https://doi.org/10.1164/rccm.201108-1562OC.
21. **Mathews L.** 2006. Paradigm shift in hemodynamic monitoring. The Internet journal of anesthesiology, vol 11. Cited: [30 November 2018]. Available at: http://ispub.com/IJA/11/2/13289.
22. **Mehta NJ, Khan IA, Mehta RN, Sepkowitz DA.** 2000. HIV-related pulmonary hypertension: analytic review of 131 cases. Chest **118:**1133–1141. https://doi.org/10.1378/chest.118.4.1133.
23. **Miyata M, Sakuma F, Yoshimura A, Ishikawa H, Nishimaki T, Kasukawa R.** 1995. Pulmonary hypertension in rats. 1. Role of bromodeoxyuridine-positive mononuclear cells and alveolar macrophages. Int Arch Allergy Immunol **108:**281–286. https://doi.org/10.1159/000237165.
24. **Mondy KE, Gottdiener J, Overton ET, Henry K, Bush T, Conley L, Hammer J, Carpenter CC, Kojic E, Patel P, Brooks JT, Investigators SUNS.** 2010. High prevalence of echocardiographic abnormalities among HIV-infected persons in the era of highly active antiretroviral therapy. Clin Infect Dis **52:**378–386. https://doi.org/10.1093/cid/ciq066.
25. **Morris A, Gingo MR, George MP, Lucht L, Kessinger C, Singh V, Hillenbrand M, Busch M, McMahon D, Norris KA, Champion HC, Gladwin MT, Zhang Y, Steele C, Sciurba FC.** 2012. Cardiopulmonary function in individuals with HIV infection in the antiretroviral therapy era. AIDS **26:**731–740. https://doi.org/10.1097/QAD.0b013e32835099ae.
26. **Oikawa M, Kagaya Y, Otani H, Sakuma M, Demachi J, Suzuki J, Takahashi T, Nawata J, Ido T, Watanabe J, Shirato K.** 2005. Increased [^{18}F]-fluorodeoxyglucose accumulation in right ventricular free wall in patients with pulmonary hypertension and the effect of epoprostenol. J Am Coll Cardiol **45:**1849–1855. https://doi.org/10.1016/j.jacc.2005.02.065.
27. **Olivetta E, Percario Z, Fiorucci G, Mattia G, Schiavoni I, Dennis C, Jäger J, Harris M, Romeo G, Affabris E, Federico M.** 2003. HIV1 Nef induces the release of inflammatory factors from human monocyte/macrophages: involvement of Nef endocytotic signals from NFκB activation. J Immunol **170:**1716–1727. https://doi.org/10.4049/jimmunol.170.4.1716.
28. **Perros F, Dorfmüller P, Montani D, Hammad H, Waelput W, Girerd B, Raymond N, Mercier O, Mussot S, Cohen-Kaminsky S, Humbert M, Lambrecht BN.** 2012. Pulmonary lymphoid neogenesis in idiopathic pulmonary arterial hypertension. Am J Respir Crit Care Med **185:**311–321. https://doi.org/10.1164/rccm.201105-0927OC.
29. **Porter KM, Walp ER, Elms SC, Raynor R, Mitchell PO, Guidot DM, Sutcliff RL.** 2013. Human immunodeficiency virus 1 transgene expression increases pulmoary vascular resistance and exacerbates hypoxia-induced pulmonary hypertension development. Pulm Circ **3:**58–67. https://doi.org/10.4103/2045-8932.109915.
30. **Rennard SI, Basset G, Lecossier D, O'Donnell KM, Pinkston P, Martin PG, Crystal RG.** 1986. Estimation of volume of epithelial lining fluid recovered by lavage using urea as marker of dilution. J Appl Physiol (1985) **60:**532–538. https://doi.org/10.1152/jappl.1986.60.2.532.
31. **Rhodes J, Udelson JE, Marx GR, Schmid CH, Konstam MA, Hijazi ZM, Bova SA, Fulton DR.** 1993. A new noninvasive method for the estimation of peak dP/dt. Circulation **88:**2693–2699. https://doi.org/10.1161/01.CIR.88.6.2693.
32. **Rusnati M, Presta M.** 2002. HIV1 Tat protein and endothelium: from protein–cell interaction to AIDS-associated pathologies. Angiogenesis **5:**141–151. https://doi.org/10.1023/A:1023892223074.
33. **Sakao S, Tatsumi K, Voelkel NF.** 2010. Reversible or irreversible remodeling in pulmonary arterial hypertension. Am J Respir Cell Mol Biol **43:**629–634. https://doi.org/10.1165/rcmb.2009-0389TR.
34. **Schweitzer F, Tarantelli R, Rayens E, Kling HM, Mattila JT, Norris KA.** 2018. Monocyte and alveolar macrophage skewing is associated with the development of pulmonary arterial hypertension in a primate model of HIV infection. AIDS Res Hum Retroviruses [Epub ahead of print]. http://doi.org/10.1089/AID.2018.0132
35. **Sitbon O, Lascoux-Combe C, Delfraissy JF, Yeni PG, Raffi F, De Zuttere D, Gressin V, Clerson P, Sereni D, Simonneau G.** 2007. Prevalence of HIV-related pulmonary arterial hypertension in the current antiretroviral therapy era. Am J Respir Crit Care Med **177:**108–113. https://doi.org/10.1164/rccm.200704-541OC.
36. **Speich R, Jenni R, Opravil M, Pfab M, Russi EW.** 1991. Primary pulmonary hypertension in HIV infection. Chest **100:**1268–1271. https://doi.org/10.1378/chest.100.5.1268.
37. **Sutendra G, Dromparis P, Paulin R, Zervopoulos S, Haromy A, Nagendran J, Michelakis ED.** 2013. A metabolic remodeling in right ventricular hypertrophy is associated with decreased angiogenesis and a transition from a compensated to a decompensated state in pulmonary hypertension. J Mol Med (Berl) **91:**1315–1327. https://doi.org/10.1007/s00109-013-1059-4.
38. **Syyed R, Reeves JT, Welsh D, Raeside D, Johnson MK, Peacock AJ.** 2008. The relationship between the components of pulmonary artery pressure remains constant under all conditions in both health and disease. Chest **133:**633–639. https://doi.org/10.1378/chest.07-1367.
39. **Torriani FJ, Komarow L, Parker RA, Cotter BR, Currier JS, Dubé MP, Fichtenbaum CJ, Gerschenson M, Mitchell CK, Murphy RL, Squires K, Stein JH, ACTG 5152s Study Team.** 2008. Endothelial function in human immunodeficiency virus-infected antiretroviral-naive subjects before and after starting potent antiretroviral therapy: The ACTG (AIDS Clinical Trials Group) Study 5152s. J Am Coll Cardiol **52:**569–576. https://doi.org/10.1016/j.jacc.2008.04.049.
40. **Yeghiazarians Y, Honbo N, Imhof I, Woods B, Aguilera V, Ye J, Boyle AJ, Karliner JS.** 2014. IL15 A novel prosurvival signaling pathway in cardiomyocytes. J Cardiovasc Pharmacol **63:**406–411. https://doi.org/10.1097/FJC.0000000000000061.